Published in final edited form as:
Biomaterials. 2012 August ; 33(23): 5776–5787. doi:10.1016/j.biomaterials.2012.04.029.

Synapse-directed delivery of immunomodulators using T-cell-conjugated nanoparticles

Matthias T. Stephan[1,2], **Sirkka B. Stephan**[2], **S. Peter Bak**[2], **Jianzhu Chen**[2], and **Darrell J. Irvine**[1,2,3,4,5,‡]

[1]Department of Material Science and Engineering, Massachusetts Institute of Technology (MIT), Cambridge, Massachusetts, USA

[2]Koch Institute for Integrative Cancer Research, MIT, Cambridge, Massachusetts, USA

[3]Department of Biological Engineering, Massachusetts Institute of Technology, Cambridge, Massachusetts, USA

[4]Ragon Institute of Massachusetts General Hospital, MIT and Harvard University, Boston, Massachusetts, USA

[5]Howard Hughes Medical Institute, Chevy Chase, Maryland, USA

Abstract

Regulating molecular interactions in the T-cell synapse to prevent autoimmunity or, conversely, to boost anti-tumor immunity has long been a goal in immunotherapy. However, delivering therapeutically meaningful doses of immune-modulating compounds into the synapse represents a major challenge. Here, we report that covalent coupling of maleimide-functionlized nanoparticles (NPs) to free thiol groups on T-cell membrane proteins enables efficient delivery of compounds into the T cell synapse. We demonstrate that surface-linked NPs are rapidly polarized toward the nascent immunological synapse (IS) at the T cell/APC contact zone during antigen recognition. To translate these findings into a therapeutic application we tested the NP delivery of NSC-87877, a dual inhibitor of Shp1 and Shp2, key phosphatases that downregulate T-cell receptor activation in the synapse, in the context of adoptive T cell therapy of cancer. Conjugating NSC-87877-loaded NPs to the surface of tumor-specific T cells just prior to adoptive transfer into mice with advanced prostate cancer promoted a much greater T-cell expansion at the tumor site, relative to co-infusing the same drug dose systemically, leading to enhanced survival of treated animals. In summary, our studies support the application of T-cell-linked synthetic NPs as efficient drug delivery vehicles into the IS, as well as the broad applicability of this new paradigm for therapeutically modulating signaling events at the T-cell/APC interface.

1. Introduction

Immune cells communicate via the formation of a receptor-containing adhesive contact zone termed an immunological synapse [1]. Upon encounter with antigen-presenting cells (APCs), T lymphocytes spatially rearrange membrane receptors, accessory molecules and downstream signaling molecules towards the T cell-APC junction to facilitate the accurate

‡Correspondence should be addressed to D.J.I. (djirvine@mit.edu).

interaction of stimulatory and inhibitory ligands with their respective receptors, to modulate T-cell expansion and, ultimately, to determine T-cell fate [2]. Therefore, regulation of these molecular interactions arises as an important therapeutic strategy to prevent pathological self-reactivity (autoimmunity) or, conversely, to boost immunity against infections or tumor cells [3]. To this end, antibodies targeting stimulatory receptors (CD28, OX-40, 4-1BB) or inhibitory molecules (e.g., PD-1) in the immunological synapse have entered advanced clinical testing [4], and an antibody blocking the inhibitory receptor CTLA-4 expressed by activated T-cells has recently received FDA approval for cancer therapy[5]. A challenge with targeting proteins involved in signaling at the IS is that these receptors may be sterically shielded from antibody or recombinant ligand therapeutics by virtue of the tight contact formed between T-cells and antigen presenting cells or target cells [6–8]. For example, CTLA-4 is sequestered in intracellular stores in T-cells and on T-cell receptor triggering, the receptor is delivered to the cell surface directly within the synapse [7, 9]. In addition, potent ligands that promote T-cell function by engaging stimulatory receptors or blocking inhibitory receptors have the potential for serious autoimmune consequences when administered systemically in a manner that allows the entire lymphocyte compartment to be stimulated [10, 11]. Thus, strategies to focus these T-cell-amplifying signals on antigen-specific cells attacking a disease target are desired to simultaneously increase the efficacy and saftey of these agents.

In parallel to efforts targeting cell surface receptors involved in T-cell stimulation, membrane-permeable small molecule compounds that can suppress or activate T-cell receptor (TCR) proximal intracellular signaling pathways have undergone preclinical and early-stage clinical evaluation [12–15]. Critical kinases, phosphatases, and adaptors involved in TCR signaling associate with receptors or lipid rafts trafficked into the IS, leading these critical intracellular signaling components to also be enriched in the synapse at the cytoplasmic face of the T-cell membrane [13, 16]. Clinical success of such synapse signaling-targeting compounds will hinge on delivering therapeutically meaningful doses of these drugs to the IS where these pathways are active. In addition, like reagents targeting receptors involved in the regulation of T-cell priming, these small-molecule drugs have potential for serious off-target as well as on-target autoimmune consequences, and their safety and efficacy will likely require a means to focus their action on disease-specific lymphocytes.

An attractive clinically-relevant setting for targeted delivery of immunomodulatory drugs to T-cells is in adoptive cell therapy (ACT). In ACT, autologous disease-specific T-cells are isolated from patients [17, 18] or generated *ex vivo* by genetic engineering [19, 20], stimulated to differentiate into potent effectors, and then reinfused into the patient to treat metastatic cancer or infectious disease [21, 22]. To enhance the efficacy of ACT, we recently showed that lipid or polymer particles in the 100–300 nm size range can be linked to T-cells via maleimidethiol conjugation without compromising cell function [23]. Using this simple *ex vivo* conjugation process, we showed that immunocytokines that promote T-cell function could be slowly released from cell-bound nanoparticles (NPs) and primarily recaptured by particle-carrying cells in autocrine signaling loops. Surface-decorating tumor-specific T cells with cytokine-loaded NPs greatly increased T-cell number, anti-tumor function, and longevity after subsequent *in vivo* transfer [23, 24].

In this study, we investigated whether, beyond providing infused T cells with autocrine sources of growth factors, covalent coupling of maleimide-functionlized nanocarriers to free thiol groups on T-cell membrane proteins could enable efficient delivery of therapeutic small-molecule drugs into the T-cell synapse. We assessed by time-lapse microscopy whether plasma membrane-anchored NPs alter their surface distribution in response to the dynamic behavior of their carrier T-cell and polarize towards the nascent immunological

synapse at the T-cell/APC contact zone, and we identified by mass spectrometry predominant anchor proteins of T cell-conjugated NPs. To evaluate the therapeutic potential of T-cell-linked synthetic NPs as drug delivery vehicles into the immunological synapse we tested the delivery of NSC-87877 [25], a small molecule dual inhibitor of Shp1 and Shp2, key phosphatases which downregulate T-cell receptor activation in the synapse [26], in the context of adoptive T-cell therapy of cancer.

2. Methods

2.1. Preparation of lipid nanoparticles

To synthesize stable maleimide-functionalized liposomes, we hydrated a dry lipid film (1.2 mg total lipids) composed of the maleimide-headgroup lipid 1,2-dioleoyl-sn-glycero-3-phosphoethanolamine-N-[4-(p-maleimidomethyl)cyclohexane-carboxamide] (MCC PE), hydrogenated soybean phosphatidylcholine (HSPC), and cholesterol (all Avanti Polar Lipids) in a molar ratio of 40:30:30, respectively, with 50 mM HEPES/150 mM NaCl-buffer pH 6.5 (500 μl) at 62°C for 2 h to form large multilamellar vesicles (MLVs). The resulting vesicles were sized by repeated extrusion at 62°C through a polycarbonate membrane (Nucleopore, Whatman, NJ) of 200 nm pore size. After extrusion, liposomes were washed with 12 ml phosphate buffered saline pH 7.4 (PBS) and collected via ultracentrifugation at 30,000 rpm for 6 hours. The liposome pellet was resuspended in 1 ml PBS and used immediately. For the preparation of fluorescent liposomes, 0.11 mg 1,1′-dioctacdecyl-3,3,3′,3-tetramethylindodicarbocyanine (DiD, Invitrogen) was admixed to the lipids before solvent evaporation. The SHP1/2 PTPase inhibitor NSC-87877 (EMD chemicals) was encapsulated in the aqueous core of liposomes by dissolving 300 μg NSC-87877 in 500 μl of the 50 mM HEPES/150 mM NaCl-lipid hydration buffer. Particle sizes were determined by dynamic light scattering on a Brookhaven 90Plus particle sizer.

2.2. Preparation of 2C effector T cells for adoptive transfer and retroviral transduction with click beetle red luciferase

Animals were housed in the MIT Animal Facility and all mouse studies were performed in accordance with protocols approved by the MIT Division of Comparative Medicine following federal, state, and local guidelines. To isolate antigen-specific T-cells, spleens of 2C TCR transgenic mice were harvested, macerated over a filter, and resuspended in ACK lysing buffer (Biosource, Rockville, MD). Effector 2C $CD8^+$ T cells were prepared by incubating splenocytes (3×10^6/mL) in complete RPMI 1640 with 1 ng/mL interleukin-7 (PeproTech, Rocky Hill, NJ) and 2 μg/mL concavalin A (Calbiochem, La Jolla, CA) at 37°C. Two days later, dead cells were removed by Ficoll gradient separation (GE Healthcare) and $CD8^+$ cells were isolated using a mouse CD8 negative isolation kit (Stemcell Technologies, Vancouver, BC).

Introduction of luciferase into T-cells for bioluminescence imaging studies was performed by retroviral transduction. Concentrated click beetle red luciferase (CBR-luc)-expressing retrovirus [27] 1 mL, kindly provided by Dr. Michel Sadelain (Memorial Sloan-Kettering Cancer Center, New York) was preloaded onto six-well non-tissue culture treated dishes coated with RetroNectin (TakiraBio) and incubated at 37°C incubation for 1 hr. An equal volume of isolated T-cells (3×10^6 cells/mL supplemented with 10 ng mIL-2/mL) was added and centrifuged at 2000 × g for 30 min). 6 hr after spinoculation, 1 mL of fresh, prewarmed RPMI, containing 10 ng mIL-2 (PeproTech, Rocky Hill, NJ) was added. T cells were used for adoptive transfer experiments 1 day after gene transfer.

2.3. Nanoparticle conjugation and in situ PEGylation

Lipid NPs were conjugated to the surface of effector T lymphocytes as previously described [23]. Briefly, 60×10^6 T cells/mL were resuspended in serum-free X-Vivo 10 medium (Cambrex, East Rutherford, NJ), mixed with an equal volume of NPs (T cell:NP ratio = 1:1000), and incubated at 37°C for 30 min with gentle agitation every 10 min. After a PBS wash to separate cells from unbound particles, residual maleimide groups present on cell-bound particles were quenched by incubation of 3×10^6 cells/mL with 1 mg/mL thiol-terminated 2KDa poly(ethylene glycol) (PEG, Laysan Bio, Arab, AL) at 37°C for 30 min in complete RPMI medium, followed by two PBS washes to remove unbound PEG.

2.4. Confocal and time-lapse videomicroscopy

We stained $CD8^+$ T cells with FITC-conjugated cholera toxin B subunit (FITC-CTB, Sigma-Aldrich, St. Louis, MO) as described previously[28]. For confocal imaging, T cells were transferred onto fibronectin (Sigma-Aldrich)-coated 10 mm teflon ring glass slides (Electron Microscopy Sciences, Hatfield, PA), fixed with 2 % paraformaldehyde, mounted with ProLong Gold Antifade reagent (Life Technologies, Grand Island, NY) for 24 hours and imaged with a Zeiss LSM 510 laser scanning confocal microscope. For cell migration analyses using time-lapse videomicroscopy we mixed cells with a collagen precursor solution (1.8 mg/mL type I bovine collagen, Advanced BioMatrix, San Diego, CA) and incubated at 37°C to allow polymerization of the solution into a fibrillar collagen gel. T-cell trans-endothelial migration imaging was performed in 24 mm diameter 3 μm pore size Transwell plates (Costar). 1×10^5 MS1 endothelial cells (ATCC) were seeded on gelatin (0.2%)-coated upper wells and allowed to grow for 2 days until confluence. We plated 1×10^5 $CD8^+$ effector T lymphocytes, conjugated with 100 DiD^+ NPs per T-cell onto confluent MS1 monolayers which had been pre-activated for 4 hr with 25 ng/mL TNF-α (Preprotech). The T-cell chemoattractant MCP-1 (10 ng/ml, Preprotech), was added to the lower wells. Cells were imaged in a 5% CO_2 humidified environmental chamber on a Zeiss Axiovert 200 inverted microscope.

2.5. Mass Spectrometry

Amine-modified polystyrene nanospheres (200 nm, Life technologies) were functionalized with maleimide groups using NHS-PEG_{24}-maleimide crosslinkers according to the manufacturer's protocol (Thermo Scientific, Rockford, IL), and were surface-coupled to 2C effector $CD8^+$ T lymphocytes as described under 2.3. 30×10^6 NP-decorated T cells were subsequently lysed in 3 ml of 9.5 M urea, 2% (w/v) CHAPS, 0.8% (w/v) Pharmalyte pH 3–10, 1% (w/v) dithiothreitol (DTT) and 5 mM Pefabloc (all Sigma-Aldrich) with vigorous vortexing, followed by 3 × 20 sec sonication (40 Watt power) on ice. To purify NPs from T-cell lysate we pelleted NPs through a 20% sucrose layer at 13.000 g for 15 minutes and washed the NP-pellet three times with distilled water. We adapted the "filter-aided sample preparation (FASP)" procedure [29] to isolate and identify proteins that became linked to maleimide-functionalized NPs during cell conjugation. Each sample was suspended in 200 μL of a solution of 8 M urea and 50 mM ammonium bicarbonate, pH 8.5. Dithiothreitol (Sigma-Aldrich) was added to a concentration of 10 mM and disulfide bonds were reduced by incubation at 60°C for 45 min. Iodoacetamide (Sigma-Aldrich) was then added at a concentration of 22 mM and cysteine thiols were alkylated by incubation at 25°C in the dark for 1 h. Urea and excess reagents were removed with a Microcon (Millipore, Billerica, MA) YM-10 10 KDa MWCO centrifugal filter device. The filtrate was discarded and 50 μL of 50 mM ammonium bicarbonate (pH 7.8) and 1 μg of trypsin (Promega, Madison, WI) were added the NPs, which remained on the Microcon filter in approximately 30–50 μL solution. Protein digestion was carried out on the Microcon filter for 16 h at 25°C. Trypsin digestion was halted by addition of 1% formic acid (Sigma-Aldrich) to lower the pH to ~3. Proteolytic peptides were then recovered by spinning the suspension through the filter; NPs and

peptides larger than those able to pass through the filter membrane remained on the filter. The filtrate volume was reduced in a vacuum centrifuge (Eppendorf, Hamburg, Germany) and the recovered peptides were analyzed by high performance liquid chromatography (HPLC) tandem mass spectrometry. A nanoflow HPLC system (Agilent 1100) with gradient elution, using a water-acetonitrile solvent system with 0.1% formic acid as the ion-pairing agent, was used to effect peptide separation on a reverse phase C_{18} Picofrit capillary column (75 μm internal diameter, New Objective, Inc.) at a flow rate of 300 nL/min. Electrospray ionization mass spectrometry was carried out on an LTQ ion trap mass spectrometer (ThermoFisher). Protein identification was carried out using the fragment ion mass spectra collected from each sample and the Sequest database search software (ThermoFisher); a mouse protein database that was generated from all mouse proteins in the Uniref protein database. Proteins were identified which had at least 90% sequence identity to database sequences. Database search results were tabulated and compared among different samples using Scaffold visualization software (Proteome Software, Inc).

2.6. In vitro T-cell expansion assays

We exposed 1×10^6 2C effector $CD8^+$ T lymphocytes to 1×10^5 irradiated (15 Gy) TRAMP-SIY target tumor cells in tissue culture–treated 24-well plates (Corning). Tumor monolayers were pretreated for 24 h with 50 ng/ml murine IFN-γ before T-cell coculture. T cells were cultured with or without 150 μM NSC-87877. No exogenous cytokines were added. On day 4, the number of viable T cells was determined by trypan blue exclusion.

2.7. Mice and orthotopic TRP-SIY prostate tumor model

Male C57BL/6 albino mice were obtained from Jackson Laboratories. Transgenic Adenocarcinoma of Mouse Prostate (TRAMP) mice expressing the 2C target antigen SIYRYYGL in the prostate (TRP-SIY mice) were previously described[30]. To enable *in vivo* longitudinal imaging of prostate tumors, we derived tumor cell clones from TRP-SIY spontaneous tumors and transduced these cells with Gaussia luciferase for imaging following orthotopic prostate implantation in congenic healthy mice: Prostate tumor-initiating stem-like cells were isolated from a primary 40-week old TRP-SIY tumor by non-adherent spheroid culture. First, the TRP-SIY tumor was dissociated by enzymatic digestion (20 μg/ml collagenase II, Gibco-Invitrogen, Carlsbad, CA) for 2 h at 37μC. Recovered cells were cultured in DMEM-F12 medium (Gibco-Invitrogen) supplemented with 20 μg/ml EGF and 10 μg/ml bFGF[31] in ultra-low adherent 6-well plates (Stemcell Technologies) for 1 week with media exchange every 2 days, leading to the growth of tumor cell spheroids.

To retrovirally tag tumor cells for bioluminescent imaging we first cloned the native Gaussia luciferase gene with the N-terminal secretion signal (pUC18 SS-Gluc, Nanolight) [32] into the oncoretroviral vector SFG [27], and plamid-transfected the pseudotyped retrovirus packaging cell line H29 [33] to generate retroviral particles. Prostate tumorspheres were then dissociated using Accutase cell detachment solution (Stemcell Technologies) and were retrovirally transduced with SFG retrovirus expressing secreted Gaussia luciferase on non-tissue culture treated dishes coated with RetroNectin. Tumor cells were subcloned by limiting dilution at 1 cell/96-well and outgrowing tumor clones were screened for sGau-luc expression by bioluminescent imaging. For orthotopic tumor cell implantation, a longitudinal incision was made in the lower abdomen of anaesthetized male C57BL/6 albino mice. The bladder, seminal vesicles and prostate were partially extravasated from the abdominal cavity to expose the dorsal lobes of the prostate. Using a 27-gauge needle, 2×10^6 TRAMP-SIY sGau-luc tumor cells were injected into each lobe in 25 μl of PBS. The abdominal cavity, muscle and skin were closed in two layers with Vicryl Rapide polyglactin 910 P-1 11 mm absorbable sutures and 7 mm stainless steel wound clips, respectively. Tumors developed over the course of ~4 weeks post implantation.

2.8. Adoptive T-cell transfer and in vivo bioluminescence imaging

Four weeks after tumor implantation, we treated mice by tail vein injection with 15×10^6 CBR-luc transduced 2C T cells and monitored *in vivo* T-cell distribution and TRP-SIY tumor burden by dual bioluminescent imaging. The following luciferins were used: Native Coelenterazine (Nanolight Technology) as a substrate for sGau-luc, resuspended in 1,2-propanediol (Sigma-Aldrich) at a concentration of 1 mg/mL and diluted to 0.25 mg/mL in sterile PBS (Life Technologies) immediately before injection. D-Luciferin (Caliper Life Sciences, Hopkinton, MA) was used as a substrate for CBR-luc, resuspended in PBS (15 mg/mL). Bioluminescence images were collected on a Xenogen IVIS Spectrum Imaging System (Caliper Life Sciences). Living Image software version 3.0 (Caliper Life Sciences) was used to acquire and quantitate the bioluminescence imaging data sets. Native coelenterazine was injected through the tail vein (5 mg/kg) into 2 % isofluorane-anesthetized animals followed immediately by 5 min acquisitions. D-Luciferin was injected (150 mg/kg) i.p. 10 min before acquisitions ranging from 10 sec to 5 min.

2.9. Flow cytometry

Anti-mouse CD8-APC and anti-CD45.1-FITC antibodies, were purchased from Ebioscience. Four days after T-cell injection, prostate tumors were resected and enzymatically dissociated in 20 μg/ml collagenase II, (Gibco-Invitrogen, Carlsbad, CA) for 2 hours at 37°C. Recovered cells were surface-stained with antibodies, washed twice with PBS and acquired on a FACSCalibur Flow Cytometer (BD Biosciences).

2.10. Statistical methods

We used the unpaired Student's t-test to test the difference between bioluminescence signals and the log-rank test to analyze survival data. All statistical analyses were performed using Prism 4.0 software.

3. Results

3.1. Linkage of MLVs to effector T-cells

Building on our prior work using cell-bound protein-loaded nanoparticles to deliver cytokines to cell surface receptors of T-cells, our strategy to modulate intracellular signaling in ACT T-cells was to link lipid vesicles loaded with membrane-permeable small-molecule drugs to the plasma membrane (Fig. 1A). For the effective retention and slow release of small-molecule drugs, we first tested whether gel-phase multilamellar lipid vesicles could be linked to $CD8^+$ effector cells using the maleimide-mediated conjugation approach we previously reported for linking lipid and polymer particles to endogenous thiols of cell surface proteins on lymphocytes. Maleimide-headgroup MCC-PE lipids incorporated into HSPC/cholesterol multilamellar vesicles (MLVs) were stable to vesicle processing at 62°C, and incubation of T-cells with MCC-functionalized MLVs led to particle linking to cells, similar to our previous findings with low-T_m lipid particles (Fig. 1B). Particles bound to T-cells were stable to repeated washing/centrifugation steps *in vitro*.

3.2. Spatiotemporal distribution of membrane-linked nanoparticles on the surface of effector T lymphocytes

To mediate their therapeutic functions, adoptively transferred T-cells need to extravasate from blood vessels into the extracellular matrix following adoptive transfer to seek and lyse tumor targets [34]. Since both events– T-cell transmigration across vasculature and the formation of lytic synapses with tumor cells –involve the large-scale reorganization of plasma membrane proteins [35], we first assessed whether plasma membrane-anchored NPs altered their surface distribution in response to the dynamic behavior of their carrier T-cell.

Confocal imaging revealed that NPs are evenly distributed on the surface of non-motile effector T cells in suspension (Fig. 1B, Fig. 2A). To track cell-bound NPs during T lymphocyte migration across endothelial barriers, we utilized an *in vitro* transwell co-culture system in which NP-conjugated effector T-lymphocytes migrate across a membrane-supported confluent endothelial monolayer in response to a chemoattractant placed in the lower chamber. Rapidly after seeding on endothelium all spherical T cells polarized to a characteristic "hand-mirror" morphology, and compartmentalized their NP pool to the uropod (Fig. 2B) likely reflecting the uropodal localization of many cell surface proteins on migrating T-cells [36]. This rearward polarization of cell surface-bound particles was also observed when T cells were seeded into 3D-collagen gels, which mimic tissue extracellular matrix and support spontaneous amoeboid T-cell motility, as visualized by time-lapse videomicroscopy (Fig. 2C).

Next, to address whether NPs remain compartmentalized at the rearward end of T-cells once they encounter cognate antigen, we imaged MLV-conjugated 2C TCR-transgenic $CD8^+$ effector T-cells engaging TRAMP prostate tumor cells, which express the target antigen of the T-cells (SIYRYYGL in the context of H-$2K^b$) [30]. Surprisingly, imaging of fixed T-cell-tumor cell conjugates after 20 min of co-incubation revealed that a majority of T-cells polarized their surface-bound NPs into the contact zone with the target tumor cell, colocalizing with GM1 ganglioside-rich membrane microdomains known to polarize into the immunological synapse [37]) (Fig. 3A, B and Table 1). To determine the dynamics of this repolarization, we imaged 2C T-cells decorated with fluorescent MLVs in time-lapse as they interacted with GFP-expressing TRAMP tumor cells in collagen gels. As T-cells contacted tumor cells, the surface-conjugated NPs were rapidly redistributed from the uropod into the nascent immunological synapse at the T-cell/APC contact zone (Fig. 3B). We confirmed that accumulation of MLVs in the immunological synapse upon contact with antigen did not interfere with target cell killing (Fig. 3C) or cytokine release by the T-cell (Fig. 3D), in agreement with our previous work using low T_m-lipid-based nanoparticles, where we found that coupling of up to ~100 particles on average to each T cell is nontoxic and does not affect key cellular functions [23]. Thus, NPs conjugated to $CD8^+$ T-cells are carried at the uropod of migrating cells but dynamically polarize to the IS during target cell recognition. However, for particle densities of at least 100 NPs/cell, translocation to the T-cell-target cell interface does not block the effector functions of killer T-cells.

3.2. Mass spectrometry characterization of nanoparticle anchor proteins in T-cell membranes

Maleimide-mediated coupling of NPs to T-cells has the advantage of allowing T-cells to be decorated by simply mixing reactive particles with the cells in the absence of additional manipulation of the lymphocytes, but in this approach the identity of the cell surface proteins to which the particles become anchored is also not known *a priori*. To identify proteins involved in anchoring of the particles to the cell surface and uncover the mechanistic basis for NP accumulation in the immunological synapse, we identified NP "anchor proteins" on T-cells by mass spectrometry. For these assays, we conjugated T-cells with maleimide-functionalized polystyrene NPs of similar size to our MLVs (200 nm diam.), which could be recovered (along with any conjugated plasma membrane proteins) following lysis of the decorated cells using sucrose gradient centrifugation. The recovered particles/proteins were washed multiple times to remove loosely attached proteins or cytosolic contaminants, then digested with trypsin. We then determined peptide mass fingerprints by LC-MS, which were matched to a protein sequence database to identify the particle-associated membrane molecules [38]. The relative frequency of distinct proteins linked to the particles was estimated by scoring the percentage of independent MS samples where each protein was robustly identified (via 3 or more unique peptide signatures) (Tables

2 and 3). Using this methodology, we found that leukocyte common antigen (CD45), a large, abundant transmembrane tyrosine phosphatase containing cysteine-rich extracellular domains [39], is a predominant membrane anchor of maleimide-functionalized NPs on T-cells (Table 2).

CD45 serves as a regulatory master switch of T-cell activation and is recruited along with the T-cell receptor into the central compartment of the early immunological synapse [40]. A second group of NP-binding membrane proteins we identified in our proteomic screen were adhesion molecules that stabilize the central signaling region of the IS [1], including the $\alpha_L\beta_2$ integrin (LFA-1) [41], adhesion molecule CD2 [42], and CD97, a receptor involved in both cell adhesion and signaling processes early after leukocyte activation [43]. Importantly, in none of 10 independent experiments were components of the T-cell receptor itself or its coreceptor CD8 identified as NP anchor proteins, which may in part explain the uncompromised antigen recognition capability of NP-decorated T cells. Beyond signaling or adhesion receptors, large highly-expressed membrane transport proteins, such as the amino acid transporter CD98 [44] and the transferrin receptor [45] were also found bound to NPs (Table 3).

Both of these carrier proteins have also been described in the literature to traffic to the immune synapse in response to TCR triggering [46, 47]. Among the group of membrane proteins without intrinsic synapse-homing properties, class I major histocompatibility complexes [48] emerged as prominent NP anchor proteins (Table 2). Also the large catalytic ATPase subunit (alpha) and a smaller glycoprotein subunit (beta) of the sodium/potassium pumps [49] were detected at high frequency (Table 3). In conclusion, these results demonstrate that maleimide-functionalized NPs conjugate to a few select anchor proteins, rather than the entire pool of proteins displayed on T-cell surfaces. Notably, the majority of the detected NP-binding molecules are known to actively translocate into the nascent immunological synapse, explaining the observed transport of cell-bound NPs to the T-cell-APC contact zone during T-cell activation.

3.3. Shp1/2 inhibitor-loaded nanoparticles for promoting TCR signaling at the immunological synapse

Adoptive cell therapy with anti-tumor T-cells represents a potent new treatment modality for patients with cancer, but tumors can render these T-cell attacks inefficient by upregulating suppressive ligands at the T-cell-tumor cell contact zone [50]. Given the synapse localization of T-cell-bound nanoparticles, we were motivated to explore the delivery of small-molecule drugs targeting critical signaling pathways active at the IS, to block negative regulatory signals delivered by tumor cells and other cells in the tumor microenvironment. To this end, we chose to focus on inhibitors of Shp1 and Shp2, key phosphatases that downregulate T-cell receptor signaling [26]. These phosphatases are recruited to the IS and activated by a host of negative regulatory signaling receptors expressed by T-cells, and in turn Shps deactivate the TCR signaling chain (Fig. 4A) [26]. We thus hypothesized that inhibition of Shp activity in the synapse would block multiple suppressive signals coming from tumor cells that would normally restrain T-cell anti-tumor activity (Fig. 4A).

NSC-87877 is a recently-described cell-permeable inhibitor of Shp-1 and Shp-2 (Fig. 4B, referred to hereafter as Shp inhibitor (ShpI)) [25]. To test the potential of ShpI for amplifying T-cell activation and tumor cell recognition, we added soluble ShpI to co-cultures of 2C T-cells and SIY-expressing prostate tumor cells, and measured the proliferation of T-cells in the presence of the drug. As shown in Fig. 4C, after 4 days of co-culture, T-cells in control untreated cultures were dying out (fold-expansion over input T-cell numbers < 1), while ShpI-supplemented cultures showed a 3.4-fold expansion in T-cell numbers, a net increase in the number of viable T-cells of ~11-fold compared to controls (p

< 0.001). Thus, Shp inhibition has clear potential to enhance the function of tumor-specific T-cells.

To minimize premature drug leakage from nanocarriers during *in vivo* transit before T-cells reach their target sites, we entrapped ShpI in the aqueous core of 200-nm maleimide-functionalized lipid vesicles, stabilized by inclusion of high T_m lipid hydrogenated soybean phosphatidylcholine (HSPC) and cholesterol. Formation of MLVs in the presence of ShpI led to encapsulation of the inhibitor with 17 ± 6 % efficiency, and the resulting MLVs slowly released the drug over a 6-day time period (Fig. 4D). As shown in the confocal micrograph of Fig. 4E, ShpI-loaded MLVs conjugated to $CD8^+$ T-cells in a manner indistinguishable from "empty" particles.

3.4. Bioluminescence-based orthotopic prostate tumor model for adoptive T-cell therapy

As a cancer with the highest rate of new cases in 2010 and the second leading cancer killer in men [51], we sought to test our approach for enhancing ACT via T cell-linked NPs *in vivo* in a model of prostate cancer. We recently described the TRP-SIY transgenic mouse model of prostate cancer, where male mice spontaneously develop orthotopic prostate tumors following puberty that express the 2C T-cell target epitope SIYRYYGL (SIY) [30]. Since tumor formation in TRP-SIY mice relies on sporadic tumor-initiating events, tumor burden can vary widely from mouse to mouse. Furthermore, longitudinal cohort studies to measure the prostate cancer volume in TRP-SIY animals rely on expensive and time-consuming magnetic resonance imaging (MRI) techniques, which precludes a reliable and accurate comparison between large treatment groups. To overcome these issues, we sought to generate TRP-SIY tumor-derived cell lines transduced with luciferase, which could be orthotopically transplanted into healthy mice to develop prostate tumors that could be monitored by bioluminescence imaging. Following a recently reported approach for enriching putative "cancer stem cells" from primary tumors [31], we isolated cells from well-developed tumors in the prostate of a 40-week old TRP-SIY mouse and placed these cells in non-adherent spheroid culture (Fig. 5A). Prostate tumorspheres expressed high levels of the pluripotency markers Nanog and SSEA-1 compared to adherent TRAMP-C2 cells, a historical prostate tumor cell line derived from TRAMP mice. We retrovirally transduced tumor cell clones isolated from these cultures with a secreted Gaussia luciferase (sGau-Luc) gene [32] (Fig. 5B) for serial bioluminescent imaging. When orthotopically transplanted into the dorsal lobe of the prostate gland of C57BL/6 mice (Fig. 5C), sGau-Luc^+ TRP-SIY tumor cells reproducibly developed into $SIYRYYGL^+$ lesions within 4-6 weeks (Fig. 5D, Supplementary Fig. 1A), which were sensitive to lysis by CD8 effector T cells from 2C TRC transgenic mice (Supplementary Fig. 1B).

3.5. Ex vivo conjugation of ShpI-loaded nanoparticles to prostate tumor-specific T-cells promotes their expansion in well-established prostate tumors

To test whether NPs carrying ShpI could enhance the expansion of T-cells in tumors by locally blocking tumor-induced suppression in the synapse, we designed experiments to simultaneously track T-cell expansion and tumor burden longitudinally using two-color bioluminescence imaging. First, sGau-Luc^+ TRP-SIY tumors were implanted orthotopically in the prostates of C57BL/6 mice and allowed to develop for 1 month. To track and quantify *in vivo* T-cell migration and accumulation in relation to tumor localization and tumor burden, we retrovirally-transduced 2C T-cells with click beetle red luciferase (CBR-luc) [27]. These luc-expressing T-cells were conjugated with ShpI-loaded MLVs *in vitro* as before prior to adoptive transfer (total drug dose of 5.1 μg ShpI per 10^6 T-cells). Four weeks post tumor implantation, we quantified sGau-Luc TRP-SIY tumor burden by bioluminescence imaging (Fig. 6A, top row), and randomly assigned mice to four groups. Two treated groups were administered 15×10^6 ShpI NP-conjugated 2C T-cells or an equal

soluble dose of ShpI (76.5 μg/animal) plus unmodified 2C T-cells. Control mice were infused with 2C T cells only or received no treatment.

Serial imaging of mice revealed that 2C T cells concurrently injected with a bolus dose of ShpI showed no difference in their ability to expand in established sGau-Luc TRP-SIY tumors relative to unmodified T cells (Fig. 6A, third row, Fig. 6B). By contrast, T cells decorated with ShpI NPs accumulated in prostate tumors at 5.7-old higher levels by day 4 post-infusion compared to T-cells supported by the same drug dose administered in an unencapsulated soluble form (Fig. 6A, third row, Fig. 6B). Quantitatively similar results were obtained by dissecting tumors 4 days after T-cell transfer and assessing the frequency of infiltrating 2C T-cells by flow cytometry (Fig. 6C). T-cells carrying ShpI-releasing MLVs showed a 5.2-fold reduction in tumor burden relative to untreated animals 10 days after T-cell transfer ($p < 0.001$), whereas tumors treated with 2C T-cells alone or 2C T-cells supported by systemic ShpI injection did not yield significant reduction in tumor burden (~1.2-fold, Fig. 6D). Further, this single adoptive cell transfer with Shp NP-carrying 2C T-cells yielded a mean 14-day survival advantage over untreated groups ($P < 0.01$), with some animals surviving 60 days longer than the last surviving control mice despite the massive tumor burden at the time of treatment (Fig. 6E). Animals treated with unmodified 2C T cells did not survive significantly longer than the no-treatment control group (median survival: 108 versus 98 days, respectively, $P = 0.16$), consistent with a poor expansion and persistence of adoptively transferred T cells in the prostate tumor tissue (Fig. 6E). Notably, ShpI NPs did not alter T-cell infiltration of tissues outside the tumor, suggesting a lack of nonspecific 2C T-cell activation at non-tumor sites. In summary, these results demonstrate that NP-mediated delivery of the suppression-blocking Shp1/2 inhibitor greatly augments the efficacy of this drug and enhances ACT therapy in this orthotopic model of prostate cancer.

4. Discussion

The contact region between a T cell and an APC represents an ideal target to therapeutically modulate immune responses since it clusters a high density of key molecules, which dictate the activation and fate of lymphocytes [52–54]. With this in mind, one central area of research and development in the tumor immunotherapy and autoimmunity fields has been to evaluate therapeutic agents for their potential to tune receptor-ligand interactions at the immunological synapse. Examples include inhibiting the PD-1/B7-H1 (PD-L1) pathway to activate anti-tumor immunity [55] or targeting the protein kinase C (PKC)-θ function in the synapse of effector T cells to treat chronic autoimmune disease [13]. Most notable, however, has been the approval of the anti-CTLA-4 antibody, Ipilimumab, by the Food and Drug Administration for the treatment of advanced melanoma [56]. CTLA-4 is a key negative regulatory receptor in T-cell activation, which is exocytosed into the synapse following TCR stimulation [9]. Despite the clinical success of Ipilimumab, the need for repeated high-dose injections to yield a modest 13% response rate [5], in combination with adverse drug reactions, illustrate the limitations of systemic infusions to target drugs into the synaptic compartment.

To safeguard against uncontrolled stimulation, T-cells cluster specific signaling receptors into spatially restricted regions of the plasma membrane, where they are positioned in proximity to respective ligands only when needed [36, 57]. Here we have exploited this mechanism as a strategy to direct drugs to their target receptors “on-demand”, by linking maleimide-functionalized nanocarriers to free thiol groups on the surface proteins of T-cells. We demonstrate that membrane-linked NPs initially cluster at the rear cell pole in motile lymphocytes, but rapidly relocate to the nascent immunological synapse following TCR activation, without perturbing normal cell function (Fig. 3). This dynamic redistribution of NPs on the T-cell surface likely reflects lateral movements of the integral membrane

proteins to which NPs are anchored within the lipid bilayer. We show that T cell-coupled nanocarriers colocalize with the TCR-signaling complex in the immune synapse only following TCR antigen recognition (Fig. 3A, B). Adoptive T-cell therapy in the clinic aims to selectively augment the function of tumor-infiltrating T cells while minimizing autoimmune toxicities of tumor/self-reactive T cells in the periphery [58, 59]. By conjugating drug-loaded NPs to tumor-specific T-cells prior to adoptive transfer, we can target potent stimulants into the immune synapse of these cells with great specificity and greatly reduced potential for off-target side effects compared to systemic drug infusions, for the implementation of safe and efficient T-cell therapy. In addition, these results explain our earlier finding that T-cells could be decorated with at most ~100–120 particles with sizes of ~200 nm before signs of interference with T-cell activation, despite the fact that in these conditions, the particles occupy only a few percent of the total T-cell surface [23]. We find that this result is not due to preferential coupling of particles to critical components of the T-cell activation machinery, but rather due to physical clustering of a majority of the particles attached to each cell into the T-cell-target cell interface during synapse formation, where they may sterically interfere with synapse assembly if present at too high a concentration.

Our rationale to deliver the Shp-1/2 phosphatase inhibitor NSC-87877 as a drug cargo into the T-cell synapse was motivated by several factors. First, Shp phosphatases are recruited into the synapse, where they deactivate key signaling molecules to terminate T-cell activation and proliferation [26]. To avoid immune recognition, cancer cells activate Shp-1/2 in tumor-infiltrating T lymphocytes by stimulating a myriad of inhibitory receptors on T-cells, such as PD-1 [14], CTLA-4 [60], TGF-β [61], or IL-10 [62] (Fig. 4A). NSC-87877 can therefore shield T cells from a multitude of tumor-derived inhibitory factors, as opposed to antibodies that block only one out of many functionally redundant receptor-ligand interactions. Secondly, protein tyrosine phosphatases inhibitors are worth exploring therapeutically as a fairly new addition to the therapeutic armamentarium of tumor immunotherapy drugs. Potent, cell permeable and highly selective Shp1/2 inhibitors have been identified by large-scale screening of compound libraries, and have not been commercially available until recently[15, 25]. Lastly, Shp1/2 -phosphatase inhibitors are ideal compounds to test the benefits of targeting a drug into the immune synapse via T-cell linked NPs, versus intravenous injections. Chronic inflammation and systemic autoimmunity are commonly-observed side effects following systemic Shp-1 inhibition [63], which has hampered the clinical testing of Shp-1 inhibitors with proven *in vitro* activities [64]. As a matter of fact, only a single low-potency Shp-1 inhibitor, sodium stibogluconate, which is an FDA-approved compound for the treatment of Leishmaniasis, is currently undergoing clinical evaluation for patients with solid tumors [12]. More recent studies, however, link systemic stibogluconate infusions to an enhanced activity of immune-suppressive regulatory T-cells, which would be the exact opposite of the desired immune-boosting outcome [65]. In contrast, stable chemical conjugation of drug-loaded NPs to the surface of T-cells provides a means for synapse-directed delivery of compounds, where tiny doses of drug can be bioactive and thereby limiting exposure of healthy tissue to toxic side effects. Beyond adoptive T-cell therapy for cancer, our studies hold promise to *in vivo* modulate synapse-driven cell fate decision of other cell types used to treat autoimmunity and transplant rejection, such as regulatory T cells or iNKT cells [66, 67], and may be applicable in other cell therapies in preclinical and clinical development [68, 69].

5. Conclusions

We show here that synthetic nanocarriers can be linked to the surface of T-cells and are actively carried to the immunological synapse by the membrane proteins to which they anchor. Surface-engineered lymphocytes deliver their NP cargo to tumor sites and concentrate drugs at the T-cell/tumor cell contact zone “on demand” following tumor

recognition. By focusing drug action only on immune cells for which they were intended, our strategy offers the tantalizing prospect of safely delivering highly potent immune stimulants.

Supplementary Material

Refer to Web version on PubMed Central for supplementary material.

Acknowledgments

This work was supported in part by the NIH (CA140476 to DJI and EB123622 to MTS), the Dept. of Defense Prostate Cancer Research Program (W81XWH-10-1-0290), and a Cancer Center Support (core) grant P30-CA14051 from the NCI. SPB is an American Cancer Society Postdoctoral Fellow (12109-PF-11-025-01-LIB). DJI is an investigator of the Howard Hughes Medical Institute.

References

1. Dustin ML, Depoil D. New insights into the T cell synapse from single molecule techniques. Nat Rev Immunol. 2011; 11(10):672–684. [PubMed: 21904389]
2. Saito T, Yokosuka T, Hashimoto-Tane A. Dynamic regulation of T cell activation and co-stimulation through TCR-microclusters. FEBS Lett. 2011; 584(24):4865–4871. [PubMed: 21110974]
3. Carreno LJ, Gonzalez PA, Bueno SM, Riedel CA, Kalergis AM. Modulation of the dendritic cell-T-cell synapse to promote pathogen immunity and prevent autoimmunity. Immunotherapy. 2011; 3(4 Suppl):6–11. [PubMed: 21524159]
4. Mellman I, Coukos G, Dranoff G. Cancer immunotherapy comes of age. Nature. 2011; 480(7378): 480–489. [PubMed: 22193102]
5. Hodi FS, O'Day SJ, McDermott DF, Weber RW, Sosman JA, Haanen JB, et al. Improved survival with ipilimumab in patients with metastatic melanoma. N Engl J Med. 2010; 19;363(8):711–723.
6. Garber K. Beyond ipilimumab: new approaches target the immunological synapse. J Natl Cancer Inst. 2011; 103(14):1079–1082. [PubMed: 21737695]
7. Pentcheva-Hoang T, Egen JG, Wojnoonski K, Allison JP. B7-1 and B7-2 selectively recruit CTLA-4 and CD28 to the immunological synapse. Immunity. 2004; 21(3):401–413. [PubMed: 15357951]
8. Pentcheva-Hoang T, Chen L, Pardoll DM, Allison JP. Programmed death-1 concentration at the immunological synapse is determined by ligand affinity and availability. Proc Natl Acad Sci U S A. 2007; 104(45):17765–17770. [PubMed: 17968013]
9. Egen JG, Allison JP. Cytotoxic T lymphocyte antigen-4 accumulation in the immunological synapse is regulated by TCR signal strength. Immunity. 2002 Jan; 16(1):23–35. [PubMed: 11825563]
10. Ponce R. Adverse consequences of immunostimulation. J Immunotoxicol. 2008; 5(1):33–41. [PubMed: 18382856]
11. Di Giacomo AM, Biagioli M, Maio M. The emerging toxicity profiles of anti-CTLA-4 antibodies across clinical indications. Semin Oncol. 2010; 37(5):499–507. [PubMed: 21074065]
12. Yi T, Elson P, Mitsuhashi M, Jacobs B, Hollovary E, Budd TG, et al. Phosphatase inhibitor, sodium stibogluconate, in combination with interferon (IFN) alpha 2b: phase I trials to identify pharmacodynamic and clinical effects. Oncotarget. 2011; 2(12):1155–1164. [PubMed: 22201704]
13. Zanin-Zhorov A, Ding Y, Kumari S, Attur M, Hippen KL, Brown M, et al. Protein kinase C-theta mediates negative feedback on regulatory T cell function. Science. 2010; 328(5976):372–376. [PubMed: 20339032]
14. Wang SF, Fouquet S, Chapon M, Salmon H, Regnier F, Labroquere K, et al. Early T cell signalling is reversibly altered in PD-1+ T lymphocytes infiltrating human tumors. PLoS One. 2011; 6(3):e17621. [PubMed: 21408177]
15. Kundu S, Fan K, Cao M, Lindner DJ, Zhao ZJ, Borden E, et al. Novel SHP-1 inhibitors tyrosine phosphatase inhibitor-1 and analogs with preclinical anti-tumor activities as tolerated oral agents. J Immunol. 2010; 184(11):6529–6536. [PubMed: 20421638]

16. Brockmeyer C, Paster W, Pepper D, Tan CP, Trudgian DC, McGowan S, et al. T cell receptor (TCR)-induced tyrosine phosphorylation dynamics identifies THEMIS as a new TCR signalosome component. J Biol Chem. 2010; 286(9):7535–7547. [PubMed: 21189249]
17. Rosenberg SA. Cell transfer immunotherapy for metastatic solid cancer--what clinicians need to know. Nature Reviews. 2011; 8(10):577–585.
18. Chapuis AG, Thompson JA, Margolin KA, Rodmyre R, Lai IP, Dowdy K, et al. Transferred melanoma-specific CD8+ T cells persist, mediate tumor regression, and acquire central memory phenotype. Proc Natl Acad Sci U S A. 2012; 109(12):4592–4597. [PubMed: 22393002]
19. Till BG, Jensen MC, Wang J, Qian X, Gopal AK, Maloney DG, et al. CD20-specific adoptive immunotherapy for lymphoma using a chimeric antigen receptor with both CD28 and 4-1BB domains: pilot clinical trial results. Blood. 2012 Epub ahead of print.
20. Brentjens RJ, Riviere I, Park JH, Davila ML, Wang X, Stefanski J, et al. Safety and persistence of adoptively transferred autologous CD19-targeted T cells in patients with relapsed or chemotherapy refractory B-cell leukemias. Blood. 2011; 118(18):4817–4828. [PubMed: 21849486]
21. Doubrovina E, Oflaz-Sozmen B, Prockop SE, Kernan NA, Abramson S, Teruya-Feldstein J, et al. Adoptive immunotherapy with unselected or EBV-specific T cells for biopsy proven EBV+ lymphomas after allogeneic hematopoietic cell transplants. Blood. 2011; 119(11):2644–56. [PubMed: 22138512]
22. Perez EE, Wang J, Miller JC, Jouvenot Y, Kim KA, Liu O, et al. Establishment of HIV-1 resistance in CD4+ T cells by genome editing using zinc-finger nucleases. Nat Biotechnol. 2008; 26(7):808–816. [PubMed: 18587387]
23. Stephan MT, Moon JJ, Um SH, Bershteyn A, Irvine DJ. Therapeutic cell engineering with surface-conjugated synthetic nanoparticles. Nature Medicine. 2010; 16(9):1035–1041.
24. Stephan MT, Irvine DJ. Enhancing Cell therapies from the Outside In: Cell Surface Engineering Using Synthetic Nanomaterials. Nano Today. 2011; 6(3):309–325. [PubMed: 21826117]
25. Song M, Park JE, Park SG, Lee do H, Choi HK, Park BC, et al. NSC-87877, inhibitor of SHP-1/2 PTPs, inhibits dual-specificity phosphatase 26 (DUSP26). Biochem Biophys Res Commun. 2009; 381(4):491–495. [PubMed: 19233143]
26. Lorenz U. SHP-1 and SHP-2 in T cells: two phosphatases functioning at many levels. Immunol Rev. 2009; 228(1):342–359. [PubMed: 19290938]
27. Stephan MT, Ponomarev V, Brentjens RJ, Chang AH, Dobrenkov KV, Heller G, et al. T cell-encoded CD80 and 4-1BBL induce auto- and transcostimulation, resulting in potent tumor rejection. Nature Medicine. 2007; 13(12):1440–1449.
28. Nam KO, Kang H, Shin SM, Cho KH, Kwon B, Kwon BS, et al. Cross-linking of 4-1BB activates TCR-signaling pathways in CD8+ T lymphocytes. J Immunol. 2005; 174(4):1898–1905. [PubMed: 15699116]
29. Wisniewski JR, Zougman A, Nagaraj N, Mann M. Universal sample preparation method for proteome analysis. Nature Methods. 2009; 6(5):359–362. [PubMed: 19377485]
30. Bai A, Higham E, Eisen HN, Wittrup KD, Chen J. Rapid tolerization of virus-activated tumor-specific CD8+ T cells in prostate tumors of TRAMP mice. Proc Natl Acad Sci U S A. 2008; 105(35):13003–13008. [PubMed: 18723683]
31. Zhang L, Jiao M, Li L, Wu D, Wu K, Li X, et al. Tumorspheres derived from prostate cancer cells possess chemoresistant and cancer stem cell properties. J Cancer Res Clin Oncol. 2012; 138(4): 675–86. [PubMed: 22237455]
32. Chung E, Yamashita H, Au P, Tannous BA, Fukumura D, Jain RK. Secreted Gaussia luciferase as a biomarker for monitoring tumor progression and treatment response of systemic metastases. PLoS One. 2009; 4(12):e8316. [PubMed: 20016816]
33. Gallardo HF, Tan C, Ory D, Sadelain M. Recombinant retroviruses pseudotyped with the vesicular stomatitis virus G glycoprotein mediate both stable gene transfer and pseudotransduction in human peripheral blood lymphocytes. Blood. 1997; 90(3):952–957. [PubMed: 9242523]
34. Shrimali RK, Yu Z, Theoret MR, Chinnasamy D, Restifo NP, Rosenberg SA. Antiangiogenic agents can increase lymphocyte infiltration into tumor and enhance the effectiveness of adoptive immunotherapy of cancer. Cancer Res. 2010; 70(15):6171–6180. [PubMed: 20631075]

35. Kasson PM, Huppa JB, Krogsgaard M, Davis MM, Brunger AT. Quantitative imaging of lymphocyte membrane protein reorganization and signaling. Biophys J. 2005; 88(1):579–589. [PubMed: 15501943]
36. Sanchez-Madrid F, Serrador JM. Bringing up the rear: defining the roles of the uropod. Nat Rev Mol Cell Biol. 2009; 10(5):353–359. [PubMed: 19373240]
37. Viola A, Schroeder S, Sakakibara Y, Lanzavecchia A. T lymphocyte costimulation mediated by reorganization of membrane microdomains. Science (New York, NY. 1999; 283(5402):680–682.
38. Nesvizhskii AI. Protein identification by tandem mass spectrometry and sequence database searching. Methods Mol Biol. 2007; 367:87–119. [PubMed: 17185772]
39. Earl LA, Baum LG. CD45 glycosylation controls T-cell life and death. Immunol Cell Biol. 2008; 86(7):608–615. [PubMed: 18607388]
40. Freiberg BA, Kupfer H, Maslanik W, Delli J, Kappler J, Zaller DM, et al. Staging and resetting T cell activation in SMACs. Nat Immunol. 2002; 3(10):911–917. [PubMed: 12244310]
41. Li D, Molldrem JJ, Ma Q. LFA-1 regulates CD8+ T cell activation via T cell receptor-mediated and LFA-1-mediated Erk1/2 signal pathways. J Biol Chem. 2009; 284(31):21001–21010. [PubMed: 19483086]
42. Espagnolle N, Depoil D, Zaru R, Demeur C, Champagne E, Guiraud M, et al. CD2 and TCR synergize for the activation of phospholipase Cgamma1/calcium pathway at the immunological synapse. Int Immunol. 2007; 19(3):239–248. [PubMed: 17220479]
43. Spendlove I, Sutavani R. The role of CD97 in regulating adaptive T-cell responses. Adv Exp Med Biol. 2010; 706:138–148. [PubMed: 21618833]
44. Komada H, Imai A, Hattori E, Ito M, Tsumura H, Onoda T, et al. Possible activation of murine T lymphocyte through CD98 is independent of interleukin 2/interleukin 2 receptor system. Biomed Res. 2006; 27(2):61–67. [PubMed: 16707844]
45. Salmeron A, Borroto A, Fresno M, Crumpton MJ, Ley SC, Alarcon B. Transferrin receptor induces tyrosine phosphorylation in T cells and is physically associated with the TCR zeta-chain. J Immunol. 1995; 154(4):1675–1683. [PubMed: 7836751]
46. Miyamoto YJ, Mitchell JS, McIntyre BW. Physical association and functional interaction between beta1 integrin and CD98 on human T lymphocytes. Mol Immunol. 2003; 39(12):739–751. [PubMed: 12531285]
47. Batista A, Millan J, Mittelbrunn M, Sanchez-Madrid F, Alonso MA. Recruitment of transferrin receptor to immunological synapse in response to TCR engagement. J Immunol. 2004; 172(11): 6709–6714. [PubMed: 15153487]
48. Flutter B, Gao B. MHC class I antigen presentation--recently trimmed and well presented. Cell Mol Immunol. 2004; 1(1):22–30. [PubMed: 16212917]
49. Tian J, Xie ZJ. The Na-K-ATPase and calcium-signaling microdomains. Physiology (Bethesda). 2008; 23:205–211. [PubMed: 18697994]
50. Gajewski TF, Meng Y, Harlin H. Immune suppression in the tumor microenvironment. J Immunother. 2006; 29(3):233–240. [PubMed: 16699366]
51. Jemal A, Siegel R, Xu J, Ward E. Cancer statistics, 2010. CA: a cancer journal for clinicians. 2010; 60(5):277–300. [PubMed: 20610543]
52. Huppa JB, Davis MM. T-cell-antigen recognition and the immunological synapse. Nat Rev Immunol. 2003; 3(12):973–983. [PubMed: 14647479]
53. Zanin-Zhorov A, Dustin ML, Blazar BR. PKC-theta function at the immunological synapse: prospects for therapeutic targeting. Trends Immunol. 2011; 32(8):358–363. [PubMed: 21733754]
54. Friedl P, den Boer AT, Gunzer M. Tuning immune responses: diversity and adaptation of the immunological synapse. Nat Rev Immunol. 2005; 5(7):532–545. [PubMed: 15999094]
55. Flies DB, Sandler BJ, Sznol M, Chen L. Blockade of the B7-H1/PD-1 pathway for cancer immunotherapy. Yale J Biol Med. 2011; 84(4):409–421. [PubMed: 22180678]
56. Mansh M. Ipilimumab and cancer immunotherapy: a new hope for advanced stage melanoma. Yale J Biol Med. 2011; 84(4):381–389. [PubMed: 22180676]
57. Valitutti S, Dupre L. Plasticity of immunological synapses. Curr Top Microbiol Immunol. 2010; 340:209–228. [PubMed: 19960316]

58. Parkhurst MR, Yang JC, Langan RC, Dudley ME, Nathan DA, Feldman SA, et al. T cells targeting carcinoembryonic antigen can mediate regression of metastatic colorectal cancer but induce severe transient colitis. Mol Ther. 2011; 19(3):620–626. [PubMed: 21157437]
59. Brentjens R, Yeh R, Bernal Y, Riviere I, Sadelain M. Treatment of chronic lymphocytic leukemia with genetically targeted autologous T cells: case report of an unforeseen adverse event in a phase I clinical trial. Mol Ther. 2010; 18(4):666–668. [PubMed: 20357779]
60. Lee KM, Chuang E, Griffin M, Khattri R, Hong DK, Zhang W, et al. Molecular basis of T cell inactivation by CTLA-4. Science (New York, NY. 1998; 282(5397):2263–2266.
61. Choudhry MA, Sir O, Sayeed MM. TGF-beta abrogates TCR-mediated signaling by upregulating tyrosine phosphatases in T cells. Shock. 2001; 15(3):193–199. [PubMed: 11236902]
62. Taylor A, Verhagen J, Akkoc T, Wenig R, Flory E, Blaser K, et al. IL-10 suppresses CD2-mediated T cell activation via SHP-1. Mol Immunol. 2009; 46(4):622–629. [PubMed: 18952289]
63. Croker BA, Lawson BR, Rutschmann S, Berger M, Eidenschenk C, Blasius AL, et al. Inflammation and autoimmunity caused by a SHP1 mutation depend on IL-1, MyD88, and a microbial trigger. Proc Natl Acad Sci U S A. 2008; 105(39):15028–15033. [PubMed: 18806225]
64. Barr AJ. Protein tyrosine phosphatases as drug targets: strategies and challenges of inhibitor development. Future Med Chem. 2010; 2(10):1563–1576. [PubMed: 21426149]
65. Iype T, Sankarshanan M, Mauldin IS, Mullins DW, Lorenz U. The protein tyrosine phosphatase SHP-1 modulates the suppressive activity of regulatory T cells. J Immunol. 2012; 185(10):6115–6127. [PubMed: 20952680]
66. Yang J, Gao L, Liu Y, Ren Y, Xie R, Fan H, et al. Adoptive therapy by transfusing expanded donor murine natural killer T cells can suppress acute graft-versus-host disease in allogeneic bone marrow transplantation. Transfusion. 2010; 50(2):407–417. [PubMed: 19788510]
67. Safinia N, Sagoo P, Lechler R, Lombardi G. Adoptive regulatory T cell therapy: challenges in clinical transplantation. Curr Opin Organ Transplant. 2010; 15(4):427–434. [PubMed: 20616725]
68. Sarkar D, Zhao W, Gupta A, Loh WL, Karnik R, Karp JM. Cell surface engineering of mesenchymal stem cells. Methods Mol Biol. 2011; 698:505–523. [PubMed: 21431540]
69. Sarkar D, Ankrum JA, Teo GS, Carman CV, Karp JM. Cellular and extracellular programming of cell fate through engineered intracrine-, paracrine-, and endocrine-like mechanisms. Biomaterials. 2011; 32(11):3053–3061. [PubMed: 21262537]

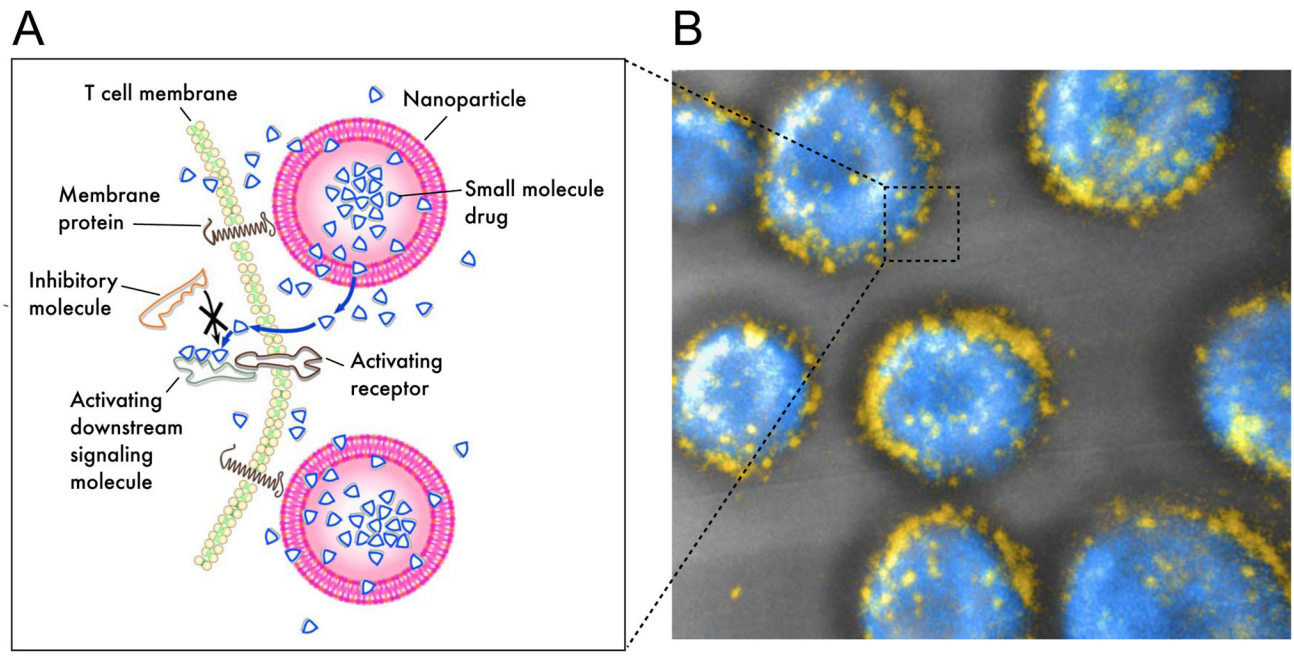

Fig. 1. Targeted release of cell membrane-permeable, immunomodulatory compounds from T-cell-linked nanoparticles

(A) Schematic view of strategy to modulate T-cell responses via nanoparticle conjugation to membrane proteins: Surface-conjugated drug-loaded nanoparticles slowly release their cargo compounds, which locally permeate the plasma membrane and block molecules in the cytosol that dampen T-cell activation. (**B**) 3D reconstruction of confocal microscopy images showing $CD8^+$ effector T-cells (CFSE stain shown in blue) immediately after conjugation with fluorescent multilamellar lipid vesicles (yellow).

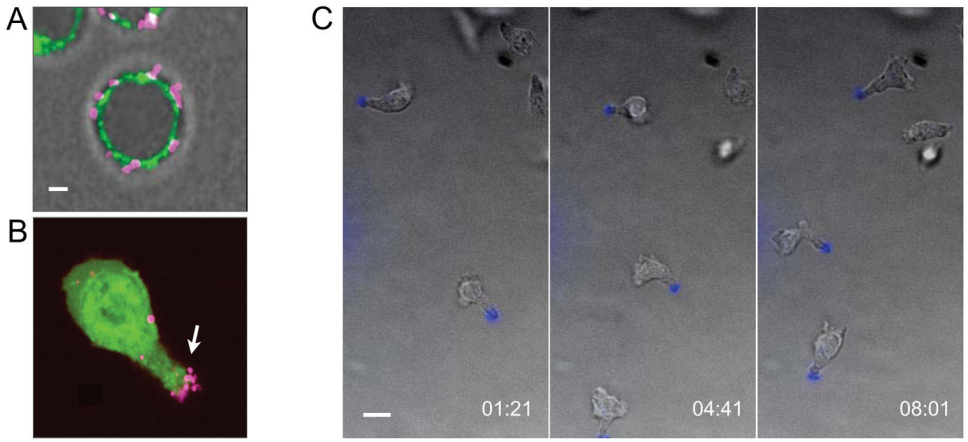

Fig. 2. Surface-linked nanoparticles cluster at the uropod of migrating T cells

(A, B) Confocal micrographs of lipid NP-conjugated $CD8^+$ effector T cells. Shown are T-cells (surface-stained with FITC-cholera toxin, green) immediately after surface-conjuation of fluorescent NPs (magenta) (**A**), or CFSE-labeled T-cells (green) conjugated with particles (magenta) migrating on an MS1 endothelial cell monolayer towards a chemoattractant (**B**). Scale bar 2 μm. (**C**) Time-lapse confocal images illustrating the polarization of surface-linked NPs (blue) towards the uropod on effector T cells migrating within a 3D collagen matrix. Scale bar: 10 μm. Times are shown in elapsed min:sec.

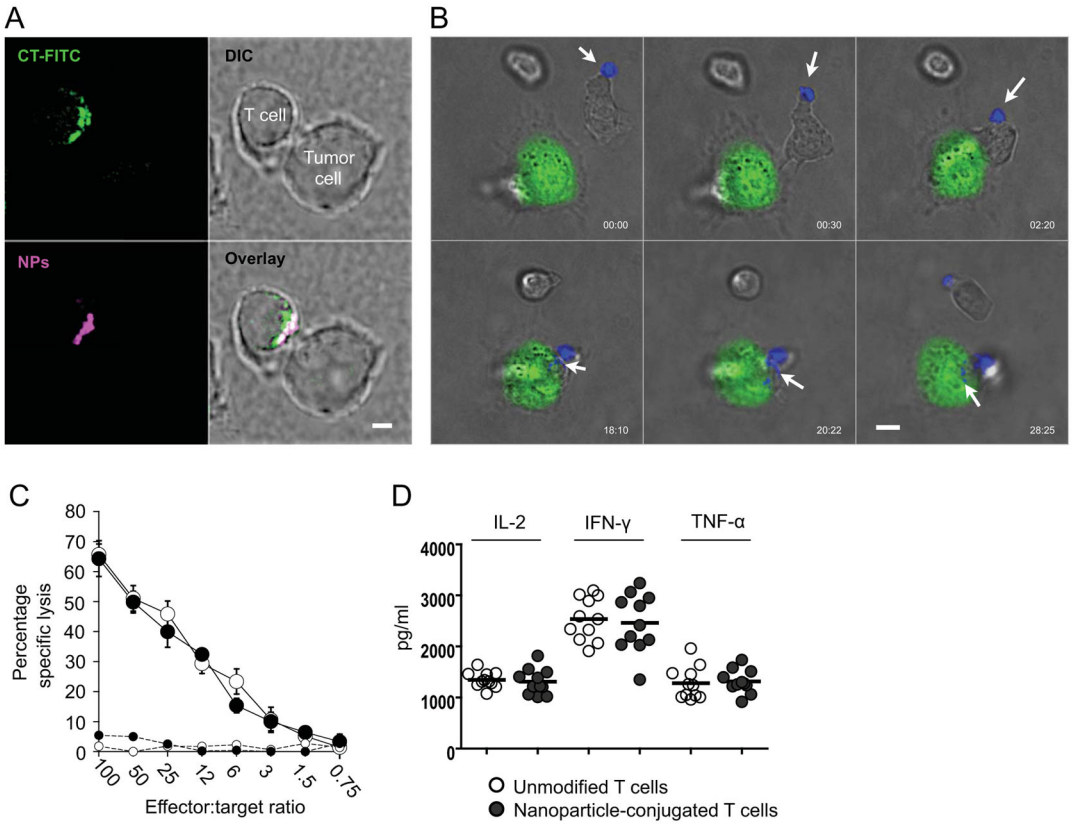

Fig. 3. Nanoparticles redistribute from the uropod into the T-cell/tumor cell contact zone without disturbing key synapse functions

(**A**) 2C $CD8^+$ effector T-cells conjugated with MLVs were incubated with SIY-target peptide-expressing TRAMP tumor cells for 20 min, then fixed and stained with FITC-cholera toxin to mark lipid rafts known to accumulate at the IS. Shown are confocal images of a T-cell forming a synaptic contact with a tumor cell. Nanoparticles were fluorescently labelled with rhodamine-conjugated lipid (magenta). Scale bar: 2 μm. (**B**) Time-lapse images illustrating the redistribution of nanoparticles (blue) from the uropod of 2C effector T cells towards the nascent synapse following TRAMP-SIY tumor target (green) recognition. Scale bar 4 μm; elapsed time shown in min:sec. (**C**) Standard 4 hour ^{51}Cr release assay comparing cytotoxicity of unmanipulated (○) and particle-conjugated (●) 2C effector $CD8^+$ T cells targeting TRAMP-SIY (large symbols) or control TRAMP (small symbols) tumor cells. (**D**) ELISA analysis of IL-2 (at 24 hrs), IFN-γ and TNF-α (at 48 hrs) secreted by NP-decorated 2C effector T-cells seeded on an irradiated TRAMP-SIY tumor cell monolayer.

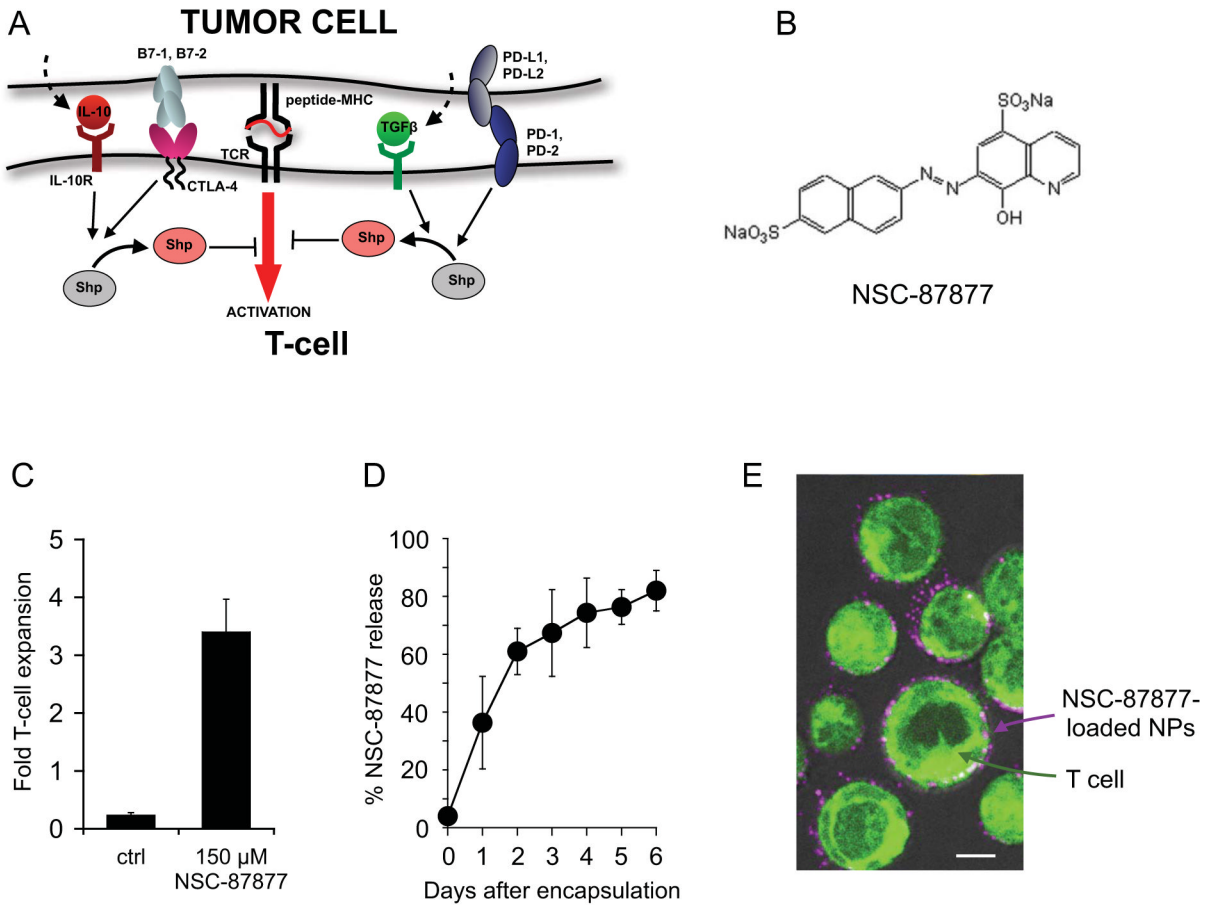

Fig. 4. Conjugation of NSC-87877-loaded nanoparticles to the surface of tumor-reactive T cells enhances their *in vitro* proliferation

(**A**) Schematic summarizing the role of Shp-phosphatases in suppressing T cell activation in the tumor microenvironment. (**B**) Molecular structure of the Shp1/2 phosphatase inhbitor NSC-87877. (**C**) Fold-expansion of 2C effector $CD8^+$ T cells cocultured on IFN-γ-pretreated TRAMP-SIY tumor monolayers in the presence or absence of NSC-87877. The number of viable T-cells was determined by Trypan blue exclusion after 4 days of *in vitro* coculture. (**D**) *In vitro* release kinetics of NSC-87877 from high-T_m lipid nanoparticles in medium containing 10% fetal bovine serum at 37°C. (**E**) Confocal micrograph of effector T cells (labeled with CellTracker Green) immediately after conjugation with maleimide functionalized NSC-87877-loaded lipid nanoparticles (magenta). Scale bar: 3 μm.

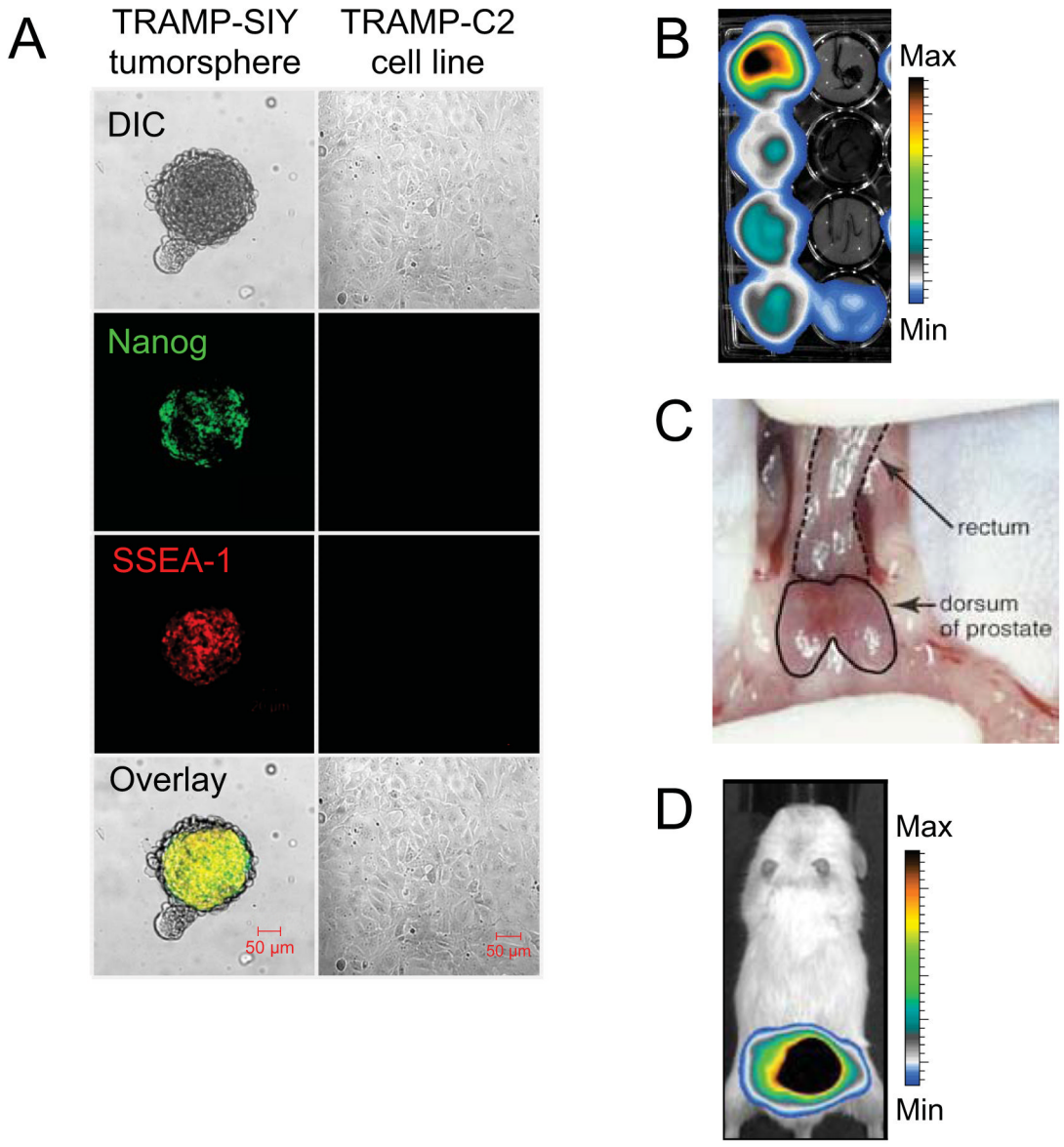

Fig. 5. Orthotopic bioluminescent mouse model of prostate cancer to evaluate the efficacy of adoptive T cell therapy

(**A**) Confocal micrographs of a tumor spheroid derived from a primary TRP-SIY tumor (left panel), compared to cells from the TRAMP-C2 cell line (right panel), stained for the stem cell markers Nanog and SSEA-1. Scale bar, 50 μm. (**B**) Selection of TRP-SIY tumor clones, stably transduced with secreted Gaussia luciferase, by bioluminescent imaging. (**C**) Orthotopic implantation of Gaussia-luciferase-positive TRP-SIY tumor cells into the dorsal lobes of the mouse prostate. (**D**) 4 weeks post-implantation, TRP-SIY tumors are visualized by *in vivo* bioluminescent imaging.

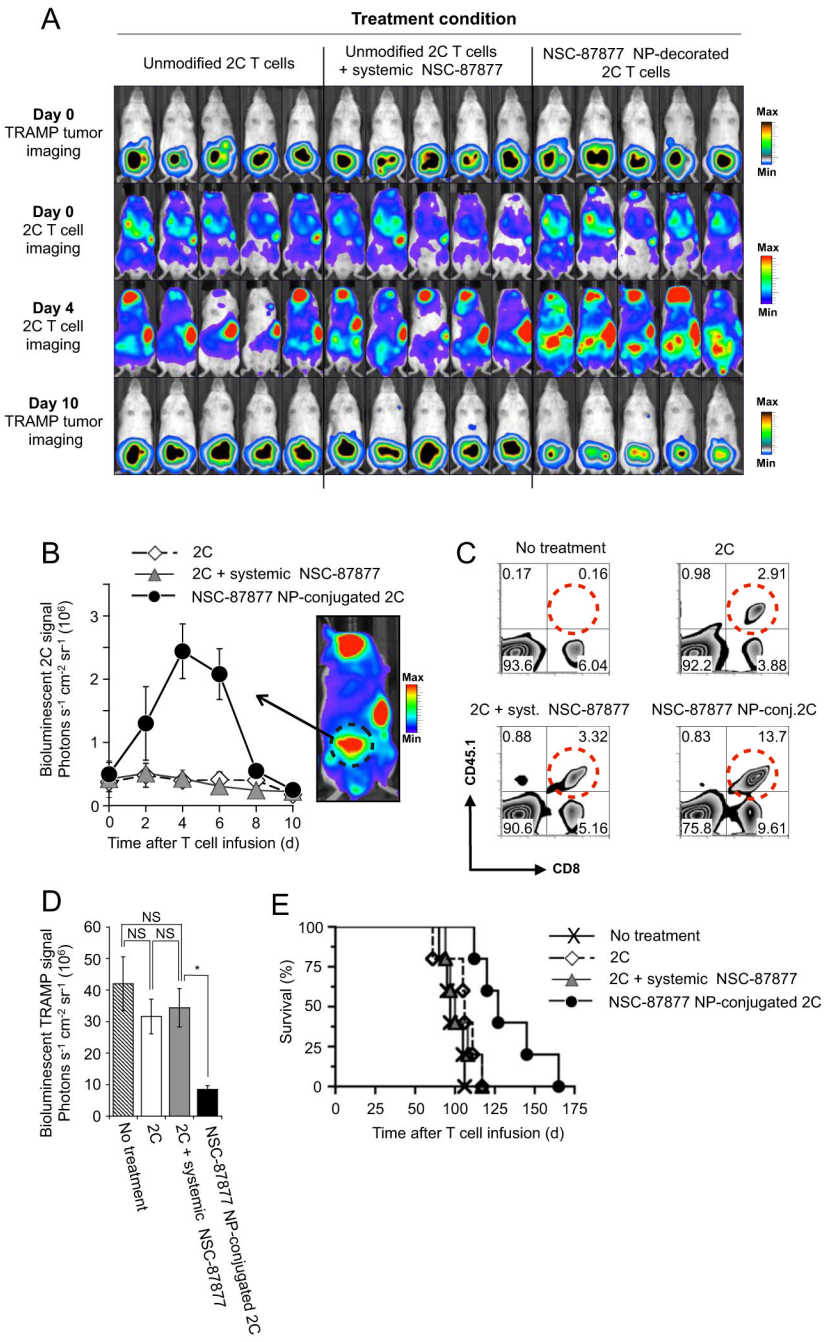

Fig. 6. ShpI-loaded NPs conjugated to the surface of tumor-specific T cells just prior to adoptive transfer enhance T-cell expansion in large established prostate tumors

Groups of mice (n = 5) bearing 4 week-established sGaussia-expressing TRP-SIY prostate tumors were treated by adoptive transfer of 15×10^6 CBR luciferase-expressing 2C T-cells alone, T-cells conjugated with MLVs carrying a total dose of 76.5 μg ShpI, or T-cells supported by an i.v. injection of an equivalent dose of soluble ShpI. (A) Dual longitudinal *in vivo* bioluminescent imaging of sGaussia-expressing tumors (top and bottom rows) and CBR-luc-expressing 2C T-cells. (B) Prostate region CBR-luc T-cell signal intensities from sequential bioluminescence imaging every 2 days after T-cell transfer. Shown are mean photon counts over time measured over the prostate area from each animal (illustrated by the

bioluminescent acquisition at right). (C) Frequencies of adoptively transferred $CD8^+CD45.1^+$ T cells recovered from resected TRP-SIY prostate tumors 4 days after T-cell transfer as detected by flow cytometry. (D) TRP-SIY tumor bioluminescent signal intensities 10 d after T cell transfer. (E) Kaplan-Meier survival curves for T-cell treated and control mice. Values shown in B and D are mean ± S.E.M.

Table 1

Frequencies of nanoparticle surface distribution observed in 50 randomly chosen T cells.

Uniform nanoparticle distribution on the surface of **resting T cells**	**n = 50/50**
Nanoparticle localization at the uropod of **migrating T cells**	**n = 48/50**
Nanoparticle redistribution into the synapse of **tumor-engaging T cells**	**n = 41/50**

Table 2

Nanoparticle binding to T-cell signaling, cell adhesion and antigen presentating membrane proteins identified by mass spectrometry.

Protein name	Accession number	Molecular weight	% experiments with >3 unique spectra
Leukocyte common antigen	CD45_MOUSE	144 kDa	90
H-2 class I histocompatibility antigen, K-D alpha chain	HA1D_MOUSE	41 kDa	60
H-2 class I histocompatibility antigen, D-D alpha chain	HA12_MOUSE	41 kDa	50
Integrin alpha-L	ITAL_MOUSE	128 kDa	40
Integrin beta-2	ITB2_MOUSE	85 kDa	40
CD97 antigen	CD97_MOUSE	90 kDa	40
T-cell surface antigen CD2	CD2_MOUSE	38 kDa	40
Extended synaptotagmin-1	ESYT1_MOUSE	122 kDa	30
Basigin	BASI_MOUSE	42 kDa	20
Transmembrane protein 173	TM173_MOUSE	43 kDa	20
Thy-1 membrane glycoprotein	THY1_MOUSE	18 kDa	20
Annexin A6	ANXA6_MOUSE	76 kDa	20
Annexin A2	ANXA2_MOUSE	39 kDa	10
Lymphocyte activation gene 3 protein	LAG3_MOUSE	57 kDa	10
Tyrosine-protein phosphatase non-receptor type 1	PTN1_MOUSE	50 kDa	10

Table 3

Nanoparticle binding to T-cell membrane carriers, pumps and channels identified by mass spectrometry.

	number	weight	with >3 unique spectra
Sodium/potassium-transporting ATPase subunit alpha-1	AT1A1_MOUSE	113 kDa	70
Sodium/potassium-transporting ATPase subunit beta-3	AT1B3_MOUSE	32 kDa	60
CD98 heavy chain	Q60849_MOUSE	59 kDa	60
Voltage-dependent anion-selective channel protein 1	VDAC1_MOUSE	32 kDa	40
Transferrin receptor protein 1	TFR1_MOUSE	86 kDa	20
Large neutral amino acids transporter small subunit 1	LAT1_MOUSE	56 kDa	20